JOURNAL OF THERMOPHYSICS AND HEAT TRANSFER
Vol. 8, No. 3, July–Sept. 1994

Examination of Theory for Bow Shock Ultraviolet Rocket Experiments—II

Deborah A. Levin* and Matthew Braunstein†
Institute for Defense Analyses, Alexandria, Virginia 22311
Graham V. Candler‡ and Robert J. Collins§
University of Minnesota, Minneapolis, Minnesota 55455
and
Gregory P. Smith¶
SRI International, Menlo Park, California 94025

In this article the radiation model, NEQAIR, used to calculate the mid-uv radiance for Bow Shock 1 and 2 flight conditions, is examined in detail. An approximate equation for the upper state NO population is derived that explains the density dependence of the calculations and sensitivity to changes in specific rates. Estimated neutral collisional excitation rates are replaced with rates based on experiment. For conditions corresponding to the two flights, the radiation obtained with an explicit treatment of the electronic excitation process was similar to that obtained from the original model. For the first time, we also test the validity of the quasi-steady-state assumption in these rarefied flows. We find that the quasi-steady-state distribution of electronic states of NO is valid for these flow conditions.

Introduction

IN the previous article,[1] we discussed the flowfield simulation, suggested changes to the baseline modeling to incorporate the effect of the work of Wray on O_2 dissociation, and compared the 230-nm NO photometer data with radiance calculations. In this article we focus on the implications of many of the key assumptions in the NEQAIR model to the results obtained in Ref. 1. The NEQAIR model[2] is used extensively by the aerothermodynamics community as a tool to model radiation in the UV. Therefore, it is crucial to determine if the discrepancy observed at slower speeds and higher altitudes can be corrected within the context of that model. Conclusions that we draw are specific to the NO molecule only, but may have implications for radiation from other molecular band systems under similar flow conditions. In this article we consider three aspects related to the modeling of NO UV radiation. First, we derive an approximate form for the NO(A) excited state population that elucidates the modeled radiation density and temperature dependence and sensitivity to specific excitation rates. Then we examine the adequacy of the empirical electronic and the estimated neutral excitation/de-excitation rates used in NEQAIR for the NO system. Lastly, we examine the validity of the quasi-steady-state assumption to the rarefied flow conditions corresponding to the second bow shock flight.

Derivation of a Simple Expression for the NO(A) Excited Electronic State Population

In Ref. 1, we showed that the agreement between theory and experiment was not complete for the second flight conditions. To separate the uncertainties in the flow and radiation modeling we consider the sensitivity of the radiation modeling to changes in temperature and density and excitation rates. To accomplish this we begin with the full set of rate equations and show that a simplified expression may be derived for the flow conditions of the first two flights. Since we are concerned with the 230-nm photometer data, we restrict our analyses to the A-state radiation. Excitation rates that couple the A and B states are small. For spectral regions at wavelengths longer than 250 nm, approximate analytic forms for the B-state radiation can be derived as well.

The baseline excitation/de-excitation processes that are modeled are

$$\mathrm{N} + \mathrm{O} + \mathrm{M} \xrightarrow{k_{Mi}} \mathrm{NO}(i) + \mathrm{M} \tag{1}$$

$$\mathrm{e}^- + \mathrm{NO}^+ + \mathrm{e}^- \xrightarrow{k^e_{ci}} \mathrm{NO}(i) + \mathrm{e}^- \tag{2}$$

$$\mathrm{NO}(i) + \mathrm{M}^* \xrightarrow{k^M_{ij}} \mathrm{NO}(j) + \mathrm{M}^* \tag{3}$$

$$\mathrm{e}^- + \mathrm{NO}(i) \xrightarrow{k^e_{ij}} \mathrm{NO}(j) + \mathrm{e}^- \tag{4}$$

$$\mathrm{NO}(i) \xrightarrow{A_{ij}} \mathrm{NO}(j) + h\nu \tag{5}$$

where M represents a third body neutral species (most likely N_2), M* is a third-body in an excited electronic state, and the indices i, j represent the X, A, and B electronic energy levels of NO. Equations (1–5) represent heavy particle and electron induced recombination, heavy particle and electron induced excitation, and spontaneous emission, respectively. The rate constants, k_{Mi} through A_{ij}, are those associated with the respective Eqs. (1–5) for the processes proceeding from left to right. The baseline model does not include any state specific information about the M or M*. The reverse rates are inferred from detailed balance

$$K_{i,eq} = \frac{[\mathrm{N}][\mathrm{O}]}{[\mathrm{NO}]} = \frac{Q_{i\mathrm{N}} Q_{\mathrm{N}} Q_{i\mathrm{O}} Q_{\mathrm{O}}}{Q_{i\mathrm{NO}} Q_{i\mathrm{NO}}} \exp\left(-\frac{D_{i0}}{kT_{\mathrm{gov}}}\right) \tag{6}$$

Presented as Paper 92-2871 at the AIAA 27th Thermophysics Conference, Nashville, TN, July 6–8, 1992; received June 16, 1993; revision received Oct. 5, 1993; accepted for publication Oct. 6, 1993.

*Research Staff Member, Science and Technology Division. Member AIAA.
†Research Staff Member, Science and Technology Division.
‡Assistant Professor, Department of Mechanical and Aerospace Engineering. Member AIAA.
§Professor, Department of Electrical Engineering.
¶Senior Research Chemist, Molecular Physics Laboratory.

where T_{gov} is the temperature that is assumed to govern the distribution of the excited electronic states; D_{i0} is the energy barrier from the ground to the ith excited state; and Q_X are the partition functions (Q_{iX}, translational, Q_X total, and Q_{iX}, the ith electronic state) for the Xth species.[3]

The distribution of electronic states is found by writing the master equation for all possible transitions

$$\frac{\dot{\rho}_i}{n_e} = -\sum_{j=1}^{m_{lev}} \left[k_{ij}^e + k_{ij}^M \frac{n_M}{n_e} + \frac{A_{ij}}{n_e} + k_{ic}^e + k_{iM} \frac{n_M}{n_e} \right] \rho_i + \sum_{j=1}^{m_{lev}} \left[k_{ij}^e + k_{ij}^M \frac{n_M}{n_e} + \frac{A_{ji} N_{jE}}{n_e N_{iE}} \right] \rho_j + \left[k_{ic}^e + k_{iM} \frac{n_M}{n_e} \right] \tag{7}$$

where the normalized population ρ_i is

$$\rho_i = \frac{N_i(T_{gov})}{N_{iE}} \tag{8}$$

and N_i and N_{iE} are the actual and equilibrium populations in the ith electronic state, respectively. The symbols n_M and n_e are the densities of neutrals and electrons in the flow, and m_{lev} is the number of electronic state energy levels (in our case, 3). N_{iE} is computed assuming that the population is in a Boltzmann distribution at the local governing temperature T_{gov}. Equation (7) represents the rate of change of the normalized population of the ith electronic state. The QSS distribution is found by assuming that this rate is slow relative to the excitation and de-excitation rates, i.e., the left side of Eq. (7) is set to zero. The effective electronic excitation temperature is defined as

$$T_{eff,i}^e = \frac{T_{gov}}{1 - \frac{T_{gov} k}{\Delta E_i} \ln\left(\frac{N_i^{QSS}}{N_{NO}} \frac{N_{NO}^{eq}}{N_{iE}} \right)} \tag{9}$$

where N_{NO} is the ground state concentration of NO predicted by the flow modeling, ΔE_i is the electronic energy of the ith electronic state, and

$$N_{NO}^{eq} = \sum_{i=1}^{3} N_{iE}$$

In Ref. 1 we discussed the reinterpretation of T_{gov} in light of the Bow Shock flight data. The baseline version of the NEQAIR model used T_v for T_{gov} in Eq. (9). Based on the comparison of theory and experiment given in Ref. 1 we found that T_{gov} is best characterized by the heavy particle translational temperature T. We continue to use that assumption for the remainder of this article.

To derive an approximate form for the NO(A) concentration, we return to Eq. (7). Examination of the various terms in Eq. (7) shows that the heavy particle collisionally induced excitation processes and radiative decay mechanisms dominate. Electron collisional rates were observed to be small because there are an insufficient number of electrons in the flow. Equation (7) can be solved explicitly for ρ_2^{QSS} since the summation extends over 3 electronic levels. Terms with products involving k_{31}^M, k_{32}^M, k_{3M}, and A_{31} were found to contribute less to the full expression than similar terms with index 2 substituted for 3. Also, with the use of Eq. (6), excitation rates may be expressed in terms of quenching processes (e.g., k_{ij}^M, $i > j$) and products of partition functions. Terms with factors of N_{iE}/N_{1E}, $i = 2, 3$ can then be neglected. After some algebraic manipulations, the QSS solution of Eq. (7) for the A state population reduces to

$$\rho_2^{QSS} \cong \frac{f N_{NO}}{N_{1E}} \tag{10}$$

where

$$f \equiv \frac{k_{21}^M}{k_{21}^M + \frac{A_{21}}{n_M} + k_{2M}} \tag{11}$$

The f factor is given in terms of the related quenching (reverse) mechanisms of Eqs. (1) and (3) and A_{21}.

The total radiation from the A state is directly proportional to

$$N_{NO} \exp\left(-\frac{\Delta E_2}{k T_{eff,2}^e} \right) = f N_{NO} \exp\left(-\frac{\Delta E_2}{kT} \right) \tag{12}$$

Hence, the magnitude of the A state contribution to the 230-nm photometer radiation is determined by the NO concentration, T and f. Equation (12) provides us with a simple physical expression from which we can derive an understanding of the relative importance of different excitation mechanisms. Substitution of Eqs. (8) and (10) into Eq. (9) gives an equivalent approximation for the effective electronic excitation temperature $T_{eff,2}^e$. Figure 1 shows an example of the spatial similarity between the full model radiation [i.e., one obtained by solution of Eq. (7)] and the approximate form given by Eq. (12). Comparisons of the exact and approximate forms of $T_{eff,2}^e$ for the conditions of the first flight at altitudes of 40, 60, and 70 km differ by less than 2%. Similar agreement was found for the second flight at 71 km. The temperature and density dependence of f changes over the range of conditions for the two flights. For the first flight at 40 km, f is approximately 0.8 in comparison with 0.07 for the second flight at 71-km altitude. For the latter case the k_{2M} rate was observed to dominate.

The temperature and density dependence of f characterizes the sensitivity of the radiation modeling to potential changes in input from the flow modeling. The temperature and density dependence of f as presently modeled in NEQAIR is given by the components of Eq. (11)

$$k_{2M} = (7.63\chi_{atom} + 3.82\chi_{molec}) 10^{-7} T^{1/2} \exp(-D_e/kT)$$

$$k_{21}^M = 4057 k T^{1/2} \sigma q[x(T)] \frac{Q_{1vJ}}{Q_{2vJ}} \frac{g_{e1}}{g_{e2}} \tag{13}$$

$$x(T) \equiv \frac{\Delta E_i}{kT}, \quad q(x) \equiv \frac{x^2 + 2.33x + 0.25}{x^2 + 3.33x + 1.68}, \quad \text{ramp function}$$

where D_e is the dissociation energy of the NO molecule (27,752.3 cm^{-1}) and χ_{atom} and χ_{molec} are the total atomic and molecular mole fractions, and Q_{ivJ} represents the molecular partition function summed over all rotational and vibrational states for the ith electronic level, g_{ei} is the ith electronic state degeneracy number, and σ is 10^{-16} cm^2. Due to the importance of the

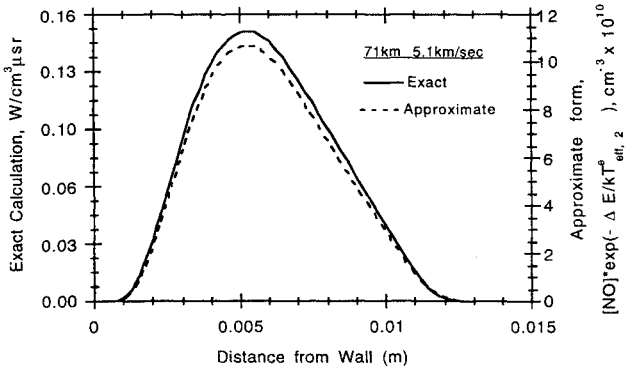

Fig. 1 Comparison of exact radiation and approximate form spatial dependence at freestream conditions of 71 km, 5.1 km/s.

k_{2M} rate at higher altitudes, an alternative expression to Eq. (13) was used from the data of Gross and Cohen[4]

$$k_{2M}^{GC} = \frac{[N][O]}{N_{2E}}\left[\frac{1.18 \times 10^{-17}}{n_M}\left(\frac{300}{T}\right)^{0.35} + 2.12 \times 10^{-34}\left(\frac{300}{T}\right)^{1.24}\right] \quad (14)$$

(It should be noted that the use of Eq. (14) for the second flight conditions requires a large extrapolation in temperature.) Figures 2 and 3 show f as a function of temperature and density for values similar to those obtained from the flow simulations. The figures show that f is more sensitive to number density than to temperature. Since the calculated total density is well established, it is unlikely that any major changes in the flow modeling will have an impact on f. The use of Eq. (14) as an alternative to Eq. (13) does not produce a significant change in f. Hence, changes in the absolute magnitude and density dependence of radiation must come from the computation of the translational temperature and the NO concentration.

The recasting of the NO(A) state concentration in terms of f provides additional insights beyond the analyses of these flight experiment data and other spectral regimes where the radiation is dominated by a finite number of strong transitions. In the limit of high densities, f approaches 1; i.e., collisional quenching dominates. At low densities, f is dominated by the spontaneous emission term, A_{21}. Hence, f is a convenient measure of the degree of deviation from Boltzmann thermal equilibrium conditions in the radiation field. When such deviations become large the explicit excitation rate values become critical.

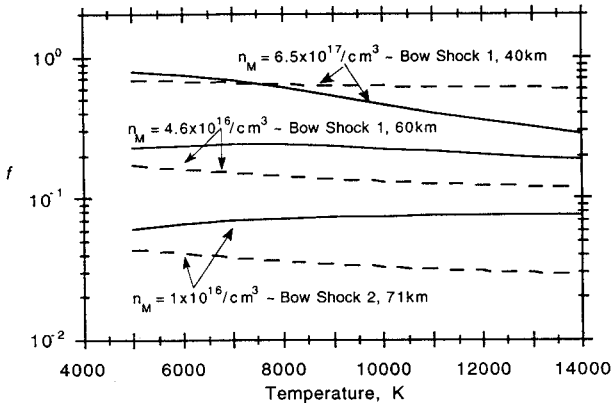

Fig. 2 Comparison of the temperature dependence of f computed using NEQAIR (solid lines) and Gross and Cohen[4] (dashed lines) rates for different flight conditions.

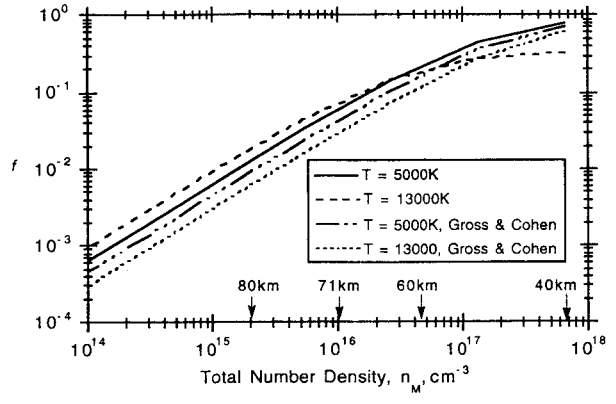

Fig. 3 Comparison of the density dependence of f computed using NEQAIR and Gross and Cohen[4] rates for different flight conditions.

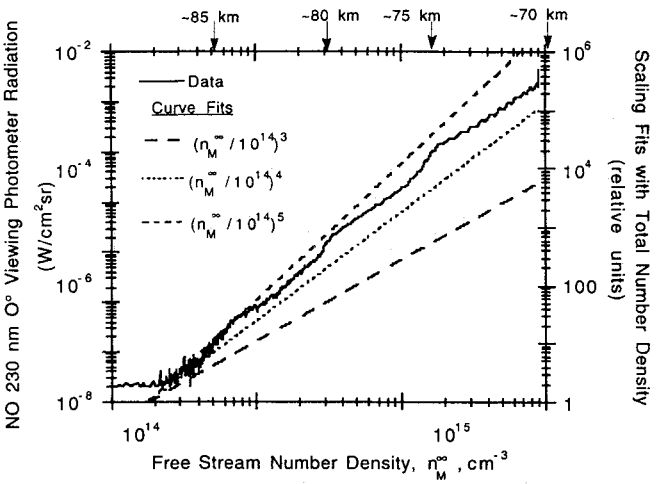

Fig. 4 Comparison of the density dependence of 230-nm forward viewing photometer data and freestream number density polynomial functions.

Finally, Eq. (12) postulates a density dependence for the observed radiation. The flow production N_{NO} is approximately fourth-order in freestream number density, and f varies between zero and first-order. Figure 4 shows a comparison of the density dependence of the 230-nm forward viewing photometer data from the second flight and polynomial functions of the freestream number density. The comparison shows that the data from the second flight deviates from a fourth-order fit which would be equivalent to Boltzmann thermal equilibrium. It also shows that the functional form suggested by Eq. (12) appears to be correct.

Replacement of Estimated Neutral Collisional Excitation Rates in the Radiation Modeling

Neutral collisional excitation processes are presently incorporated in the model in the manner[2] given by Eq. (13). High temperature measurements of some of these rates have been obtained[5,6] since the original formulation of the radiation model. To examine this further, we have replaced Eqs. (1–4) with explicit excitation processes that have intermolecular electronic state coupling. An alternative form of Eq. (7) is then used to solve for the electronic state distribution in NO and the radiance in the 230-nm spectral region. We compare the 230-nm forward viewing spectral radiance as a function of altitude obtained with these new rates to the results computed with the Wray flow modeling (see Fig. 6 of Ref. 1). Inclusion of this more detailed excitation chemistry in the radiation modeling will test the adequacy of the baseline modeling, and lay the groundwork to examine other quantities of interest, such as radiation from other excited states of NO or radiation from other emitters in the flow.

The excitation processes and forward rates that will be used to derive a new form of the master equation are summarized in Table 1. The table lists the forward excitation rates in the usual Arrhenius form

$$k_{fi} = AT^n \exp(-\Delta E/kT) \quad (15)$$

and for those rates fit to data, the temperature range where measurements were obtained. It should be noted that none of the data for direct excitation of NO are reported for temperatures greater than 4500 K, which is considerably below temperatures predicted by the flow modeling for the second flight. Table 1 (Refs. 7–10 and 14, cited therein) represents an updated version of rate data originally compiled by Smith et al.,[6] who considered the relevant chemical reactions and rates for the production of NO(A) in shock heated air. The reverse reaction rate constants k_{ri} are calculated from the forward rates by detailed balance.

Table 1 Fundamental excitation rates

Indices	Reaction	Forward rate constants A[a]	n	E, erg	Tested range, K	Ref.
1	$N + O \rightarrow NO(A)$	8.64×10^{-17}	−0.35	0.0	300–2,000	4
2	$N + O + M \rightarrow NO(A) + M$	2.48×10^{-31}	−1.24	0.0	300–2,000	4
3	$N + N \rightarrow N_2(A)$	8.14×10^{-17}	−0.35	0.0	Not applicable	7
4	$N + N + M \rightarrow N_2(A) + M$	1.27×10^{-27}	−1.6	0.0	8,000–15,000	8
5	$N + N_2 \rightarrow N_2(A) + N$	1.53×10^{-2}	−2.23	1.0×10^{-11}	8,000–15,000	8
6	$N_2(A) + NO \rightarrow NO(A) + N_2$	6.64×10^{-11}	0.0	0.0	Not applicable	9
7.1	$N_2(A) + O_2 \rightarrow N_2 + O_2$	2.32×10^{-12}	0.0	0.0	Not applicable	10
7.2	$N_2(A) + O \rightarrow N_2 + O$	2.91×10^{-11}	0.0	0.0	Not applicable	10
7.3	$N_2(A) + N \rightarrow N_2 + N$	4.88×10^{-11}	0.0	0.0	Not applicable	10
8.1[b]	$NO(A) + N_2 \rightarrow NO + N_2$	1.15×10^{-11}	0.5	9.7×10^{-13}	500–4,500	11
8.2	$NO(A) + O_2 \rightarrow NO + O_2$	9.24×10^{-12}	0.5	0.0	500–4,500	12
8.3	$NO(A) + O \rightarrow NO + O$	3.06×10^{-11}	0.5	0.0	500–4,500	12
8.4	$NO(A) + NO \rightarrow NO + NO$	1.69×10^{-11}	0.5	0.0	1,350–2,460	13
9	$NO(A) \rightarrow NO + h\nu$	4.7×10^{7}	0.0	0.0	Not applicable	14

[a]Units are in (cm^3/molecule/s) or (cm^6/molecule^2/s). [b]See text.

Since the time of Smith's work,[6] new data for reactions (8,1) through (8,4) have been reported. For the flow regimes of both flights, the $NO(A) + N_2 \rightarrow NO + N_2$ reaction (8,1 of Table 1) is important and will be shown to control a great deal of the excitation processes in the radiation modeling. For many of the temperature and density values relevant to the two flight regimes, the associated reverse reaction is the largest excitation mechanism for formation of NO(A). One uncertainty that is associated with reaction (8,1) is the energy dependence in its cross section that is used at temperatures higher than the data fit. We report and use here the larger of the rate constant expressions recommended by Smith,[12] and based on the relatively sparse but suggestive data in Refs. 5, 11, and 13. The other uncertainty is related to the branching ratio of excited to ground state products. The reactions as written and implemented in our treatment assume that the products are in the ground state. The products of quenching are formed in states and levels that rapidly equilibrate with the thermal populations, and thus that detailed balance may be used for reverse rates. The actual branching ratios and importance of relaxation processes are not well known. Reaction (8,3) is a theoretical result reported by Smith[12] based on an extension of a theoretical model successfully applied to other NO quenching reactions.[11]

The amount of NO(A) is found by writing out the new master equation, assuming that the predominant coupling is between N_2, $N_2(A)$, N, O, NO, and NO(A). This will give two coupled first-order differential equations for $d[NO(A)]/dt$ and $d[N_2(A)]/dt$

$$\begin{Bmatrix} \frac{d[NO(A)]}{dt} \\ \frac{d[N_2(A)]}{dt} \end{Bmatrix} = \begin{bmatrix} b_{11} & b_{12} \\ b_{21} & b_{22} \end{bmatrix} \begin{Bmatrix} [NO(A)] \\ [N_2(A)] \end{Bmatrix} + \begin{bmatrix} a_1 \\ a_2 \end{bmatrix} \quad (16)$$

where

$$a_1 = [N][O](k_{1f} + k_{2f}[M]) + \sum_{i=1}^{4} k_{8,ir}[M]_i[NO] \quad (17)$$

$$b_{11} = -\left\{k_{1r} + k_{2r}[M] + k_{6r}[N_2] + \sum_{i=1}^{4} k_{8,if}[M]_i + k_{9f}\right\} \quad (18)$$

$$b_{12} = k_{6f}[NO] \quad (19)$$

$$a_2 = [N][N]\{k_{3f} + k_{4f}[M]\} + k_{5f}[N][N_2] \sum_{i=1}^{3} k_{7,ir}[M] \quad (20)$$

$$b_{21} = k_{6r}[N_2] \quad (21)$$

$$b_{22} = -\left\{k_{3r} + k_{4r}[M] + k_{5r}[N] + k_{6f}[NO] + \sum_{i=1}^{3} k_{7,if}[M]_i\right\} \quad (22)$$

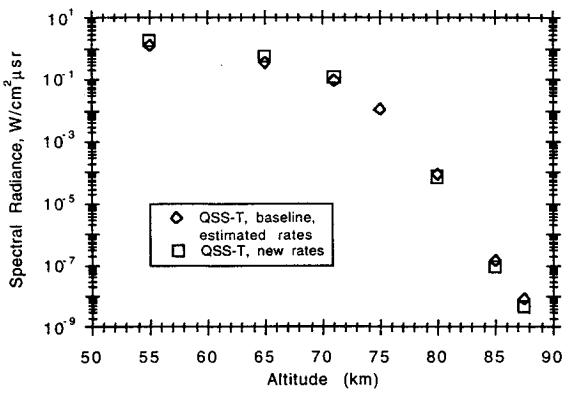

Fig. 5 Comparison of the QSS-T (baseline, estimated rates) and QSS-T (with new rates) for simulation of the 230 nm, 0 deg-viewing radiances a function of altitude.

and k_{if} and k_{ir} refer to rate constants given in Table 1, and unless otherwise indicated, the ground electronic state is assumed. The indices used in Eqs. (17–22) correspond to those given in Table 1, and $[M]_i$ is the concentration of the quencher associated with the $(7, i)$ or $(8, i)$-th process. In the quasisteady state, the left side of Eq. 16) is set to zero to obtain

$$[NO]_{qss} = \frac{(a_1 b_{22} - b_{12} a_2)}{(b_{12} b_{21} - b_{11} b_{22})} \quad (23)$$

Substitution of $[NO(A)]_{qss}$ into Eq. (9) then gives the electronic excitation temperature and the spectral radiance from the gamma band system.

Comparisons of simulations of the 230-nm, 0-deg viewing photometer radiance using the QSS-T model and the QSS-T with new rates model are as follows. For the first flight both models gave the same results. As mentioned earlier, however, the flow conditions in the second flight are more difficult to model. Figure 5 shows the new results, "QSS-T (new rates)" compared with the QSS-T calculation given in Fig. 4 of Ref. 1. They are seen to be nearly identical.

Inclusion of the excitation mechanisms given in Table 1 would seem to provide additional DOF to a complex model; yet, the results remain nearly the same. To understand this, a connection with the original radiation modeling is made by rederiving Eqs. (10) and (11) for the rates in Table 1. The terms which involve new pathways not included in Eqs. (1–5) are b_{22}, b_{12}, b_{21}, and a_2. If we ignore these terms in the expression for $[NO(A)]_{qss}$ (which is actually a good approximation for the first flight conditions, since $b_{22}{*}b_{11} \gg b_{12}{*}b_{21}$

and $a_1{*}b_{22}$ is usually larger than $b_{12}{*}a_2$), we are left with the expression

$$[\mathrm{NO(A)}]_{\mathrm{qss}} \cong a_1/b_{11} \tag{24}$$

Substitution of Eqs. (17) and (18) into Eq. (24), with retention of the largest contributions and the assumption of detailed balancing, gives

$$[\mathrm{NO(A)}]_{\mathrm{qss}} \cong \frac{k_{8.1f}[\mathrm{N_2}][\mathrm{NO(A)}]_{\mathrm{eq}}}{k_{8.1f}[\mathrm{N_2}] + k_{1r} + k_{2r}[\mathrm{N_2}] + k_{9f}} \tag{25}$$

Dividing the numerator and denominator by $[\mathrm{N_2}]$ and setting it equal to n_M, a good approximation under the present conditions, we have

$$f_{\mathrm{new}} = \frac{k_{8.1f}}{k_{8.1f} + k_{9f}/n_M + k_{1r}/n_M + k_{2r}} \tag{26}$$

This has the same density functional form as Eq. (11) with $k_{8.1f} = k_{21}^M$; $k_{9f} = A_{21}$; and, $k_{1r}/n_M + k_{2r} = k_{2M}$. The f_{new} factor of Eq. (26) has nearly the same number density dependence as the f factor with the Gross and Cohen[4] rates shown in Fig. 3.

Overall, the inclusion of detailed excitation processes and experimentally determined rates gives as good an agreement with experiment as before. Of course, the new expression for $[\mathrm{NO(A)}]_{\mathrm{qss}}$ includes other terms which introduce new processes and values that under other flow conditions may be important or give different results.

Validity of the QSS Approximation to Bow Shock 1 and 2 Flights

The quasi-steady-state assumption is questionable at the rarefied flow regimes of the second flight and its validity has never been tested in these rarefied flow regimes. At these conditions, the rate of population of the NO excited states may be similar to the rate of fluid motion; if this occurs, the QSS model will break down. The production and destruction rate equations for population of the NO, X, A, and B electronic states can be summarized as a system of coupled differential equations of first-order

$$\dot{\boldsymbol{\rho}} = \boldsymbol{C}\boldsymbol{\rho}(t) + \boldsymbol{b} \tag{27}$$

where $\boldsymbol{\rho}(t)$ is a vector representing the normalized population. The $\boldsymbol{C}$ and $\boldsymbol{b}$ matrices, which are computed in NEQAIR, represent appropriate summations over electronic, neutral, and radiative production and loss terms as given in Eq. (7). For the ground state, conservation of total population is assumed

$$\rho_1 = \frac{N_{\mathrm{NO}} - (\rho_2 N_{2E} + \rho_3 N_{3E})}{N_{1E}} \tag{28}$$

If Eq. (28) is substituted into Eq. (27), the system of three coupled differential equations can be reduced to two:

$$\dot{\boldsymbol{\rho}} = \boldsymbol{C}'\boldsymbol{\rho}(t) + \boldsymbol{b}' \tag{29}$$

By further algebraic manipulations, a second-order nonhomogeneous differential equation with constant coefficients that are functions of temperature, density, and excitation rates can be obtained for $\rho_2(t)$. Constants of integration are obtained from the two initial boundary conditions:

$$\begin{aligned} \rho_2(t = 0) &= 0 \\ \dot{\rho}_2(t = 0) &= b_2' = \frac{C_{21}N_{\mathrm{NO}}}{N_{1E}} + b_2 \end{aligned} \tag{30}$$

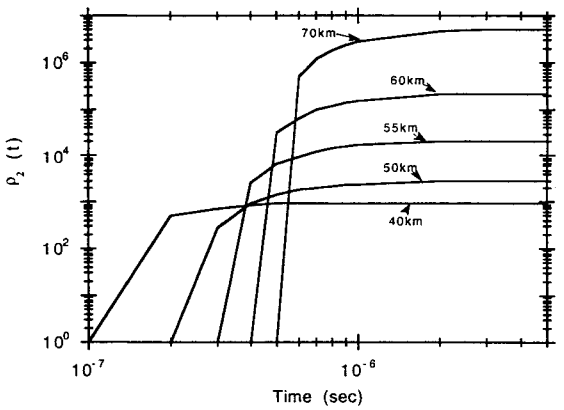

Fig. 6 Comparison of time dependence for $\rho_2(t)$ at the location of peak radiation along the stagnation streamline for a speed of 3.5 km/s.

Expressing ρ_2 as the sum of the particular (QSS) and homogeneous solutions gives

$$\begin{aligned} \frac{\rho_2^{(t)}}{\rho_2^{\mathrm{QSS}}} &= 1 - \exp(\alpha_1 t)\left[1 + \frac{b_2'}{(\alpha_1 - \alpha_2)\rho_2^{\mathrm{QSS}}} - \frac{\alpha_1}{(\alpha_1 - \alpha_2)}\right] \\ &\quad - \exp(\alpha_2 t)\left[\frac{\alpha_1}{(\alpha_1 - \alpha_2)} - \frac{b_2'}{(\alpha_1 - \alpha_2)\rho_2^{\mathrm{QSS}}}\right] \end{aligned} \tag{31}$$

where α_1 and α_2 are the nondegenerate roots of the associated quadratic equation and are negative. Analytic relationships for ρ_3 follows in a similar manner. Figure 6 shows solutions of Eq. (31) computed for trajectory conditions corresponding to the first flight. The figure shows that the time constant increases as density decreases; however, even at 60 km there are sufficient collisions to reach steady state by about 1.0 μs. Compare this with a typical flow time on the order of 20 μs. Thus, the radiative time constant is fast relative to flow transport.

Again, it is useful to derive an approximate, simpler form of Eq. (31) to determine the dominant processes. It was found that for the first flight trajectory conditions, Eq. (31) could be simplified to

$$\begin{aligned} \frac{\rho_2^{(t)}}{\rho_2^{\mathrm{QSS}}} &\cong 1 + e^{C_{22}'t} - 2e^{C_{33}'t} \\ C_{22}' &= -n_M\left[k_{21}^M + k_{23}^M + k_{2M} + \frac{A_{21}}{n_M}\right] \\ C_{33}' &= -n_M\left[k_{31}^M + k_{32}^M + k_{3M} + \frac{A_{31}}{n_M}\right] \end{aligned} \tag{32}$$

where A_{21} and A_{31} are the Einstein transition probabilities (8.6 and 1.5 $\times$ 10^6 s^{-1}, respectively). Equation (32) shows that in the limit of small density, the time constants approach the Einstein A coefficients. When collisional processes are fast relative to flow time scales, the electronic excitation temperature $T_{\mathrm{eff},i}^e$ is less sensitive to the excitation rates than to the governing temperature. This is consistent with the f factor sensitivity to temperature, density, and excitation rate values.

The results shown in Fig. 6 provide insight regarding the time constants that are implied by Eq. (10). To compare these time constants directly to those in the flow modeling, it is necessary to extend the above analysis. Under the assumption that the flow and radiation calculations are decoupled, the conservation equation for ρ_i along a streamline can be expressed as

$$\frac{\partial \rho_i}{\partial t} + u\frac{\partial \rho_i}{\partial \xi} = w_i \tag{33}$$

where u is the velocity along the streamline direction ξ, and w_i is the ith electronic state source term.

For steady flow conditions $\partial\rho_i/\partial t$ in Eq. (33) is zero, and the source terms are given by the right side of Eq. (29). Thus

$$u\frac{\partial\rho_2}{\partial x} = b_2 + C_{22}\rho_2 + C_{23}\rho_3$$
$$u\frac{\partial\rho_3}{\partial x} = b_3 + C_{32}\rho_2 + C_{33}\rho_3 \tag{34}$$

Equation (34) is solved using a finite difference approach. The present method is computationally intensive and unoptimized. Convergence was checked by reducing the grid size.

Comparisons between the exact and QSS-derived temperatures and populations for flow conditions at 71 and 80 km at 5.1 km/s were made. These cases were chosen to be at sufficiently low densities to warrant testing the applicability of the quasi-steady-state approximation. Figure 7 shows a comparison of the electronic excitation temperature for the A and B states of NO in the quasisteady state and the exact solution for conditions of 5.1 km/s, 71 km. The exact and approximate solutions are essentially the same for both the A and B states. The small differences will have minimal affect on the computed radiance. The improved formulation given by Eq. (34) permits computation of the excitation temperature through the shock front. The normalized populations are shown for the same flowfield case in Fig. 8. Figures 9 and 10 show comparisons of the exact and QSS solutions for the excitation temperatures and normalized populations at conditions of 5.1 km/s 80 km. Even with the decreased density, the exact and QSS solutions are the same for the A and B states. In view of this agreement, the QSS model, which is dependent on the flow residence time being long compared to the electronic

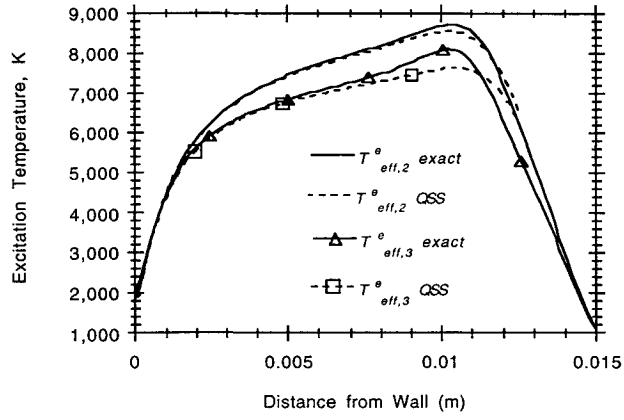

Fig. 7 Comparison of quasisteady state and exact electronic excitation temperature solutions at 5.1 km/s, 71 km.

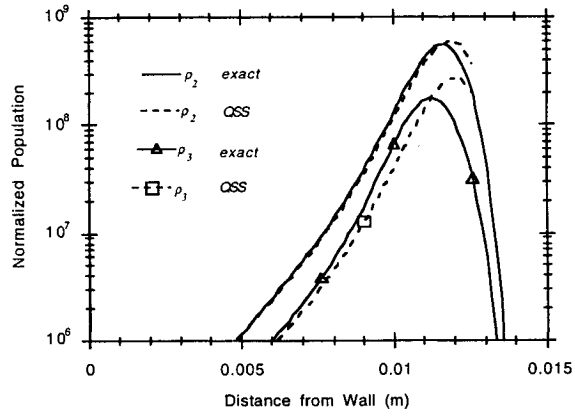

Fig. 8 Comparison of quasisteady state and exact electronic excitation normalized population solutions at 5.1 km/s, 71 km.

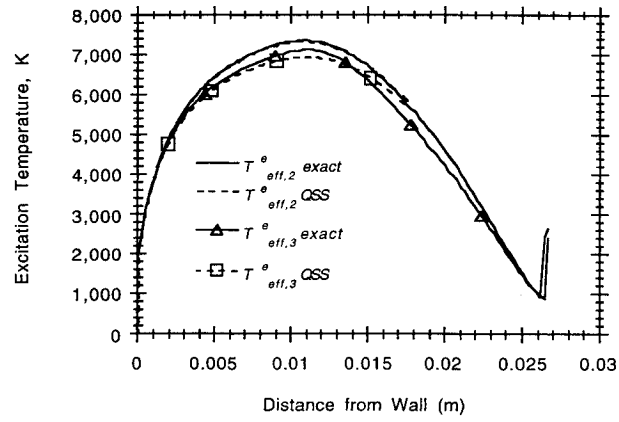

Fig. 9 Comparison of quasisteady state and exact electronic excitation temperature solutions at 5.1 km/s, 80 km.

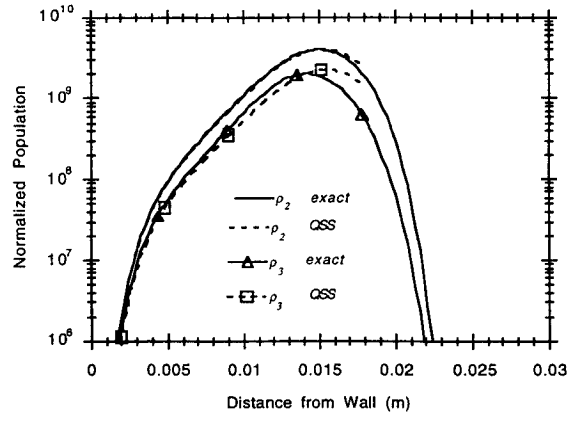

Fig. 10 Comparison of quasisteady state and exact electronic excitation normalized population solutions at 5.1 km/s, 80 km.

excitation time constants, may continue to be used in the density regime of the second flight.

Conclusions

Examination of the radiation model has provided a number of insights to our understanding of the 230-nm spectral region. Although the NEQAIR model is sufficiently general to account for excitation by electrons and neutral particles, only the latter processes contribute for the flight regimes of the bow shock ultraviolet (BSUV) experiments. The sensitivity study shows that the NO(A) state radiation predictions can be expressed simply in terms of three rate constants with a simple density dependence. With the assumption of microscopic reversibility, the temperature dependence of the f factor is understandably weak.

It has been shown that the QSS approximation agrees with exact solutions of upper state populations and effective excitation temperatures in these flight regimes for the present modeling rates. These results suggest that the QSS assumption continues to remain valid at these altitudes for the γ- and β-band contributions which dominate the radiation in the spectral bandpass of the 230-nm photometer (230 ± 25 nm).

Therefore, the types of corrections to the radiation model that would most likely affect the radiation would have to involve large changes to the neutral collisional excitation rates or their temperature dependence.

References

[1]Levin, D. A., Candler, G. V., Collins, R. J., Erdman, P. W., Zipf, E. C., and Howlett, C. L., "Examination of Theory for Bow Shock Ultraviolet Rocket Experiments—I," *Journal of Thermophysics and Heat Transfer*, Vol. 8, No. 3, 1994, pp. 447–452.

[2]Park, C. "Calculation of Nonequilibrium Radiation in the Flight Regimes of Aero-Assisted Orbital Transfer Vehicles," *Thermal Design of Aero-Assisted Orbital Transfer Vehicles*, Vol. 96, edited by H. F. Nelson, Progress in Astronautics and Aeronautics, AIAA, New York, 1985.

[3]Park, C., *Nonequilibrium Hypersonic Aerothermodynamics*, Wiley, New York, 1990.

[4]Gross, W. F., and Cohen, N., "Temperature Dependence of Chemiluminescent Reactions. II. Nitric Oxide Afterglow," *Journal of Chemical Physics*, Vol. 48, No. 6, 1968, pp. 2582–2588.

[5]Meier, U. E., Raiche, G. A., Crosley, D. R., Smith, G. P., and Eckstrom, D. J., "Laser-Induced Fluorescence Decay Lifetimes of Shock-Heated NO(A)," *Applied Physics B.*, Vol. 53, 1991, pp. 138–141.

[6]Smith, G. P., Crosely, D. R., and Eckstrom, D. J., "Interim Assessment—Mechanism and Rate Constants for the Chemistry of Radiating, Shock-Heated Air," SRI International, SRI Rept. MP 89-037, Menlo Park, CA, Feb. 1989.

[7]Young, R., and Black, G., "Excited State Formation and Destruction in Mixtures of Atomic Oxygen and Nitrogen," *Journal of Chemical Physics*, Vol. 44, No. 10, 1966, pp. 3741–3751.

[8]Shui, V. H., Appleton, J. P., and Keck, J. C., "Three-Body Recombination and Dissociation of Nitrogen: A Comparison Between Theory and Experiment," *Journal of Chemical Physics*, Vol. 53, No. 7, 1970, pp. 2547–2558.

[9]Piper, G. C., Cowles, L. M., and Rawlins, W. T., "State-to-State Excitation of NO($A\ ^2\Sigma^+$, $\nu' = 0, 1, 2$) by N_2($A\ ^3\Sigma_u^+$, $\nu' = 0, 1, 2$)," *Journal of Chemical Physics*, Vol. 85, No. 6, 1986, pp. 3369–3378.

[10]Golde, M. F., "Reactions of N_2($A\ ^3\Sigma_u^+$)," *International Journal of Chemical Kinetics*, Vol. 20, 1988, pp. 75–92.

[11]Thoman, J. W., Jr., Gray, J. A., Durant, J. L., Jr., and Paul, P. H., "Collisional Electronic Quenching of NO($A\ ^2\Sigma^+$) by N_2 from 300 to 4500 K," *Journal of Chemical Physics*, Vol. 97, No. 11, 1992, pp. 8156–8183.

[12]Smith, G. P., private communication, Menlo Park, CA.

[13]Gray, J. A., Paul, P. H., and Durant, J. L., "Electronic Quenching Rates for NO($A\ ^2\Sigma^+$) Measured in a Shock Tube," *Chemical Physics Letters*, Vol. 190, Nos. 3 and 4, 1992, pp. 266–270.

[14]Zacharias, H., Halpern, J. B., and Welge, K. H., "Two Photon Excitation of NO($A\ ^2\Sigma^+$, $\nu' = 0, 1, 2$) and Radiation Lifetimes and Quenching Measurements," *Chemical Physics Letters*, Vol. 43, 1976, pp. 41–44.